

3-D Surface Segmentation of Free-Form Objects using Implicit Algebraic Surfaces

Rachid Benlamri and Yousuf Al-Marzooqi

Department of Computer Engineering,
Etisalat College of Engineering
Po. Box 980, Sharjah, United Arab Emirates
e-mail: benlamri@ece.ac.ae

Abstract. This paper describes a new technique for free-form object segmentation from a single arbitrary-viewed range image. The aim is to derive a surface description of objects that may vary in shape and complexity without any restriction on the type of surfaces on the object. We propose a surface representation scheme that uses edge information to build a surface description using algebraic implicit surfaces. The proposed technique, not only reduces the number of used patches, but also preserves surface-depth and orientation continuity. This is done by propagating and blending piecewise hermite interpolation surfaces. The system has been tested on several synthetic and real range images and the experimental results have shown that the system can produce reliable surface description of a variety of free-form objects.

1 Introduction

The computer vision community faced with the limited scope of simple geometric models, see free-form representations as the key to solve complex 3-D recognition tasks from structured light sensors such as laser range finders or stereo depth images [1,2]. A free-form surface is the one that has a well defined surface normal that is continuous almost everywhere except at vertices, edges and cusps [2]. Human faces and sculptures are typical examples of free-form objects. Although much progress has been made in the field of 3-D vision and object recognition [2], it is widely accepted that reliable segmentation and recognition of arbitrary viewed complex curved objects is still a challenging task [2]. This is mainly due to shape complexity, existing noise, and occlusion effects [2]. Many techniques for free-form object segmentation were proposed. The most successful were those combining edge and region information [3-6]. Typically, edge-based techniques, which attempt to extract closed boundaries of components by detecting discontinuity in both depth and surface orientation, present difficulties when dealing with incomplete broken edges [5]. Region based techniques on the other hand, attempt to cluster surfaces based on their intrinsic differential geometric properties [1], but, also present difficulties when dealing with occlusion and surface continuity at the boundaries. This is because differential geometry is a theory for smooth differentiable surfaces, while free-form objects are not entirely smooth but piecewise smooth. In this paper we combine edge and region information to recover from these problems. A surface-curvature operator

is applied to extract valuable edge information that is used in turn to control the surface-fitting process.

The segmentation process consists of three main stages. First, an edge map is extracted from the range image using a surface-curvature operator, and edge points are classified into jump boundary, creases, and extrema curvature (smooth edges). The edge map is then thresholded and skeletonized to produce one-pixel wide edge curves. Second, the labeled edge map is used as the basis to generate dense triangular meshes for surface fitting. The surface triangulation is then restructured into a graph based on triangle-adjacency criterion. Finally, spanning trees, consisting of triangles with similar differential geometric properties, are extracted from the graph. The spanning trees are used to form larger homogeneous surface components. To ensure piecewise surface continuity and to avoid problems related to occlusions, crossing surfaces and hollow objects, surface continuity and differentiability conditions are used to progressively merge neighboring triangles while preserving reliable surface interpolations. Typically, larger surface patches are generated by propagating piecewise hermite interpolation surfaces along triangles belonging to the same spanning tree. These are then blended along cross edges linking neighboring spanning trees. To avoid surface orientation discontinuities, surface blending is applied only at cross edges that link surfaces separated by smooth edge curves. This method reduces significantly, the number of used surfaces for object representation while preserves surface-depth and orientation continuity.

The rest of the paper is organized as follows. Section 2 describes the curvature-based edge detection algorithm. In section 3, the technique used for surface fitting is presented. The experimental results are discussed in section 4, and finally, conclusions from the work are drawn and further research work is suggested.

2 Edge Detection

Edge detection techniques for range images are intended to localize discontinuities in both depth and surface orientation. The aim is to extract closed boundaries of object components [7]. Typically, most edge detection techniques for range images have used local surface properties such as surface curvature and surface normal to describe 3-D shape [1, 4-9]. Surface curvature is the rate at which the surface deviates from its tangent plane, and since it is invariant to viewing directions and does not change with occlusion [7], this is used as the main feature for segmenting range images. The edge detection technique used in this study searches mainly for jump and crease boundaries by computing respectively, at every image point, zero-crossings and extrema of surface curvature in some chosen directions.

Prior to edge detection, the range image is first smoothed to reduce the effect of noise. The smoothing process is very important since the calculation of curvature involves second-order partial derivatives and hence may significantly magnify the effects of noise. Consequently, noise is removed by convolving the image with a rotationally invariant Gaussian mask. Once smoothing is performed, the directional surface curvature $k_{\phi}(p)$ along direction ϕ , given by:

$$k_{\phi}(p) = -\frac{f_{\phi}''}{(1 + f_{\phi}'^2)^{3/2}} \left[\frac{1 + (A \cos(\phi) - B \sin(\phi))^2}{1 + A^2 + B^2} \right]^{1/2} \quad (1)$$

where:

f_{ϕ}' : is the first-order directional derivative of f

f_{ϕ}'' : is the second-order directional derivative of f

$A = f'(0^{\circ})$

$B = f'(90^{\circ})$

is computed in the four main directions (0° , 45° , 90° , 135°) [3,4]. The largest curvature $k_{\phi}(p)$, among the four obtained values, is used to compute zero-crossings and extrema. Typically, jump boundaries where surface depth are discontinuous, create zero-crossings of the curvature in a direction normal to that of the boundary [4]. A zero crossing is given by a zero surrounded by non-zero numbers of opposite sign on the two sides, or by a sequence of two numbers of opposite sign. Creases and curvature extrema where surface normals are discontinuous cause a local extremum of the curvature at that point. Crease differs from curvature extremum by being steep extremum, that is an extremum with high slopes of curvature values in both of its sides, in a direction normal to that extremum. Creases may also create zero-crossings away from the location of the boundary itself [4]. Zero-crossings and extrema are thus used to classify edge points. The resulting edge map is then thresholded and skeletonized to yield one-pixel wide edge curves. Finally, a curve-linking process within a threshold of 5 pixels is performed. Fig.1. shows some of the edge detection results obtained using the above described technique.

3 Surface Fitting

The study of geometric and topological properties of 3-D surfaces has been of great importance to the computer vision community [1-2, 10-11]. A variety of geometric models such as parametric surfaces [10,11], algebraic implicit surfaces [12,13], superquadrics [14,15], and generalized cylinders [2] among others, have been used to describe 3-D shape for object recognition purposes. Most of these methods were application dependent, aiming to design an object model for use in a specific vision application. The challenge, however, consists of developing a model that is general enough to represent free form objects regardless of domain [2]. In this paper, an attempt is made towards this direction. The proposed technique is based on algebraic implicit surfaces for a number of reasons that are justified below. An algebraic surface can be defined implicitly as the zero-set of an arbitrary function f as shown below.

$$S = \{(x, y, z) \mid f(x, y, z) = 0\} \quad (2)$$

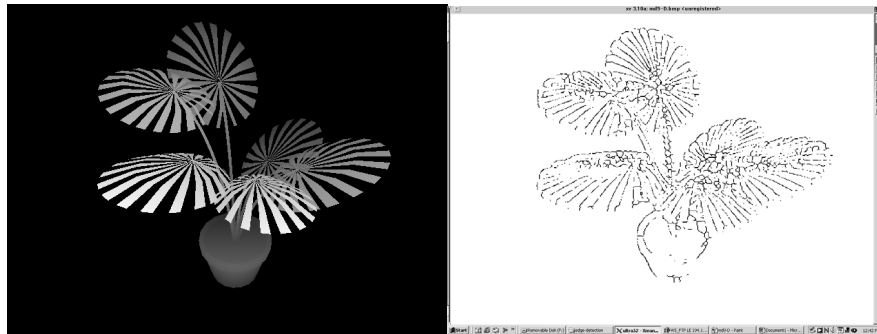


Fig. 1. Edge detection results

The classical and most used least squares fitting of an algebraic surface to data, is to minimize the algebraic distance over the set of given 3-D discrete data sample, that is [16]:

$$e_{algebraic} = \sum_{1 \leq j \leq m} (f(x, y, z))^2 \tag{3}$$

Unfortunately, the classical least squares fitting algorithm is limited by the stability of the fitting process. “Fitting a surface to an order greater than 4 can produce surfaces whose shape matches poorly to the object from which the data were obtained”[2]. This is mainly due to: i) local inconsistency with the surface orientation continuity of the data set; ii) local over-sensitivity of the polynomial zero-set around the data to small data perturbation; and iii) instability of the coefficients due to excessive degrees of freedom in the polynomial. Mathematically, this problem is referred to as the Runge problem [16]. It is exhibited by the oscillation problems between data points when using Lagrange interpolation. One solution to this problem is to substitute the algebraic distance with Euclidian distance, and to change the way the interpolation is carried out. Hermite interpolation, where the first derivative of the polynomial is controlled in addition to the value of the polynomial at each given point, has proven to converge properly for all continuous functions when the number of sampling points and thus the degree of the polynomial increases. Hence, Piecewise Hermite Interpolation Surfaces (PHISs) are more flexible to approximate a complex surface while achieving higher order of smoothness. Moreover, they present a number of advantages over parametric surfaces with regard to their applicability to: i) unbounded surfaces which are mainly caused by object occlusion, ii) surfaces that contain holes such as the case of hallow objects, and iii) unordered 3-D local surface data caused by either noise or non-homogeneously spaced data points [16]. However, the main shortcoming held against the use of algebraic implicit surfaces is that the representation being multivalued may cause the real zero contour surface to have multiple sheets, self-intersections and several other undesirable singularities [17]. A solution to this problem, using the Bernstein-Bezier (BB) form of a trivariate polynomial, consists of introducing a sufficient criterion for the BB form within a tetrahedron such that the real zero-contour of the polynomial is smooth (non-singular) and a single sheeted algebraic surface [17]. This solution was adopted in this work to construct cubic surfaces that interpolate 3-D data.

Prior to surface fitting, range data is organized into triangular meshes. Surface triangulation is very crucial to any reliable surface reconstruction [1]. This is due to the fact that the problem is not limited to finding a smooth interpolant, but concerns the estimates of some geometric properties such as curvature and extraction of elementary shapes to recover 3D objects [18]. This is why the proposed triangulation uses the extracted edge points as initial sets for surface triangulation. The triangulation is then completed by generating additional triangles using a set of rules to preserve topological properties of object surfaces. The applied rules are:

1. Connect every two points where edge curves exist.
2. Connect the two points with the shortest Euclidian distance (shorter line first). This rule selects proximate triangle vertices for best fit.
3. Do not connect any two points with a line that crosses any existing edge curve. This rule avoids crossing edge-curves and hence, minimizes surface depth and orientation discontinuities.
4. Do not connect two points where the Euclidian distance is significantly greater than the average distance over a small neighborhood. This rule minimizes the effect of noise.

Dense triangular meshes are built based on the rules mentioned above. The surface triangulation is then transformed into a triangle-adjacency graph G , as shown in Fig.2. In a such graph, the vertices represent the triangles and an edge (i,j) in the graph means that triangles T_i, T_j are adjacent. Four different types of triangle-to-triangle adjacency may result from such graph. These are those sharing: i) a non-edge segment; ii) jump-edge segment; iii) crease-edge segment; and iv) curvature extremum edge segment. These are respectively labelled 0, 1, 2 and 3.

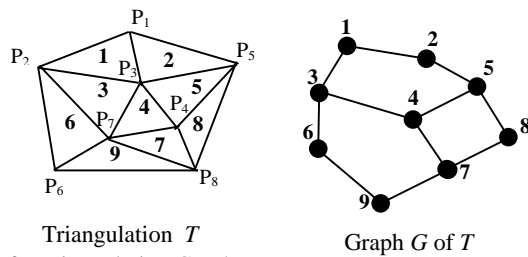


Fig. 2. Example of a Triangulation Graph

Triangles are approximated by smooth piecewise hermite interpolation surfaces. A surface $f = 0$ interpolates a triangle $I=(i,j,k)$ if it interpolates the three vertices (p_i, p_j, p_k) of I [19], so that:

1. $f(p_m) = 0$ for $m = i, j, k$
2. $\nabla f(p_m) = c_m n_m$, for some nonzero constants c_m , where:

$$\nabla f(p_m) = \left(\frac{\partial f}{\partial x}, \frac{\partial f}{\partial y}, \frac{\partial f}{\partial z} \right)^T (x_m, y_m, z_m), \quad m = i, j, k, \tag{4}$$

The interpolation surface $f(p)=0$ is a cubic surface written in Bernstein-Bezier (BB) form (for more details about the BB form, see [11,19]). To construct such a function, we first add a new point, p_l , such that the three tangent planes at point p_i, p_j, p_k are locally contained in tetrahedron $H = [p_i p_j p_k p_l]$ [17]. The function $f(p)$ is defined by:

$$f(p) = \sum_{|\lambda|=3} c_\lambda B_\lambda^n(\alpha) \tag{5}$$

If we let $c_{3000} = 0, c_{0300} = 0, c_{0030} = 0$, then we obtain:

$$f(p_m) = 0, \text{ for } m = i,j,k \tag{6}$$

Moreover, for $m = i,j,k$, if we choose:

$$c_{2e_m+e_n} = \frac{c_m}{3} (p_n - p_m)^T n_m, \text{ for } n=i,j,k,l, n \neq m \tag{7}$$

where: c_m is a nonzero constant. We then obtain [11]:

$$\nabla f(p_m) = c_m n_m \tag{8}$$

The cubic interpolation surface $f(p)=0$ as determined above interpolates the triangle vertices p_i, p_j, p_k with given normal directions n_i, n_j, n_k .

Let us now consider two adjacent triangles, $I_1=(i,j,k)$ interpolated by the cubic surface $f_1 = 0$, and triangle $I_2=(i,j,l)$, so that the shared segment (i,j) is not an edge segment, which enforces the surface continuity precondition along their joint curve. The cubic surface $f_2 = 0$, interpolating I_2 and which results from the propagation of f_1 with G^1 -continuity is constructed by considering the cutting plane $p_{ij} = 0$ so that:

$$f_2 = f_1 - (ax + by + cz + d) p_{ij}^2 \tag{9}$$

It can be seen that $f_2 \in (f_1, p_{ij}^2)$, the ideal generated by f_1 and p_{ij}^2 . Also, surface $f_2=0$ meets $f_1 = 0$ with G^1 -continuity along the plane $p_{ij} = 0$. To ensure that $f_2 = 0$ interpolates point p_l with normal direction $n_l = (n_{lx}, n_{ly}, n_{lz})$, let:

$$\begin{aligned} f_2(p_l) &= 0 \\ \frac{\partial f_2(p_l)}{\partial x} n_{ly} - \frac{\partial f_2(p_l)}{\partial y} n_{lx} &= 0 \\ \frac{\partial f_2(p_l)}{\partial x} n_{lz} - \frac{\partial f_2(p_l)}{\partial z} n_{lx} &= 0 \\ \frac{\partial f_2(p_l)}{\partial y} n_{lz} - \frac{\partial f_2(p_l)}{\partial z} n_{ly} &= 0 \end{aligned} \tag{10}$$

Thus we get a system of linear equations in a, b, c, d . Considering the linear dependence of the last three equations, there will remain a free coefficient which can be used as a shape parameter.

Since surface propagation should not be performed across triangles sharing edge curves, a surface propagation graph G_p is extracted from G by removing edges with

labels 1, 2, and 3 from graph G . This may result into a graph, G_p , broken down into a number of connected sub-graphs representing smooth continuous surface patches. For each sub-graph $G_{p_{i=1..r}}$, where r is the number of connected sub-graphs, the following procedure is applied to propagate surface patches interpolating triangles belonging to that sub-graph, G_{p_i} , into a larger surface, denoted by S_{p_i} .

1. Choose arbitrarily an element $I_{0i} \in T$ and construct an interpolation cubic surface f_{0i} for I_{0i} which is set as an initial surface.
2. Generate a spanning tree T_i with I_{0i} as a root.
3. Start from I_{0i} , for any edge (I_k, I_l) in the tree T_i , construct a propagation surface as described earlier.

After constructing all smooth continuous surfaces $S_{p_{i=1..r}}$, we then start blending surfaces that share curvature extrema (smooth) edges. This is done by constructing blending surfaces of degree five from those surfaces sharing edge segments labelled 3 in the graph $G - \{\cup G_{p_{i=1..r}}\}$. This process ensures that surfaces are blended if and only if they share a curvature extremum edge, that is an extremum with low slopes of curvature values in both of its sides, in a direction normal to that extremum. To blend two cubic surfaces patches, $f_1 = 0$ and $f_2 = 0$, sharing a smooth edge (i,j) , we consider p_1, p_2 : two cutting planes, both containing the line $p_i p_j$. The surface G defined by [20]:

$$G = (1 - u)f_1 p_2^{n+1} - u f_2 p_1^{n+1} = 0, \quad 0 < u < 1 \tag{11}$$

is the blending surface that joins the two cubic surfaces $f_1 = 0, f_2 = 0$ with G^n -continuity along $p_1=0, p_2=0$ respectively. Fig.3. shows an example of surface blending.

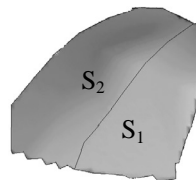


Fig. 3. Surface Blending along Smooth Edges

Once surface blending is completed, the surface description of the scene is finalized by identifying those adjacent surfaces sharing crease edges (labeled 2) from the refined graph.

4 Experimental Results

In order to show the performance of the present system, several experiments were carried out on both noisy synthetic and real range images. Range images are captured using a digital stereo head device which consists of two progressive scan CMOS greyscale imagers with a resolution of (1288 x 1032) pixels. For image rendering purpose, the average greylevel (taken from the correlated stereo image) of the vertices

spanning each triangle is used for line drawing of surface triangulation. Similarly, the generated surfaces are rendered using greylevel taken from the correlated stereo image. Fig.4. shows the surface segmentation results of a noisy synthetic image. Fig.4.a shows the computed stereo depth image while Fig.4.b shows the edge detection results. The surface triangulation, which is built from the edge map, is shown in Fig.4.c and the surface fitting results are presented in Fig.4.d. It can be seen from Fig.4.b that a reliable edge map is extracted, showing most of the boundaries of the horse's mane which have low depth values. The extracted edge map is successfully used to build a precise triangulation as shown in Fig.4.c. Finally, Fig.4.d shows the results of the surface fitting process.

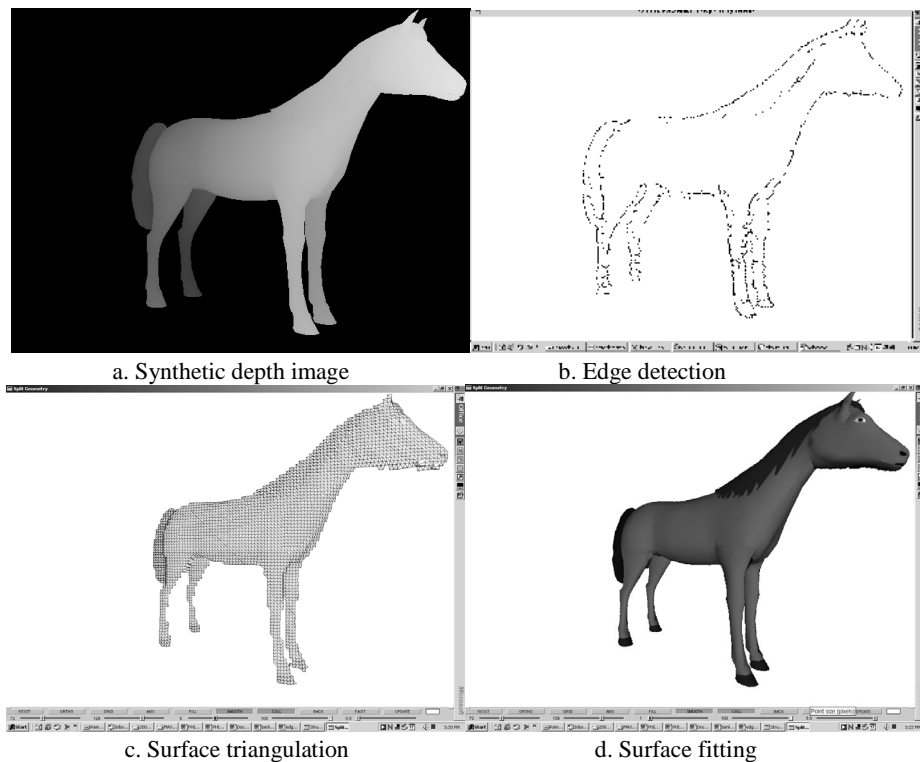


Fig. 4. Surface Fitting Results for a Synthetic Range Image

The results in Fig.5, which consist of a real range image, show some of the limitations of the proposed segmentation technique. It can be seen from Fig.5.c that incorrect triangulation may result from occlusion effects. Although, the results reported in Fig.5.b show that the employed edge detection technique is not too sensitive to occlusion as demonstrated by the accurate segmentation of most occlusions resulting from the overlapped plant leaves. However, if a single occlusion defect is reported, this will lead to over-segmentation. In this case, a defect is shown from the occlusion of one of the leaves with the pot (located on the right side of the scene). This may be due to noise at the jump boundaries. This occlusion defect has in turn affected the surface triangulation as clearly shown in Fig.5.c.

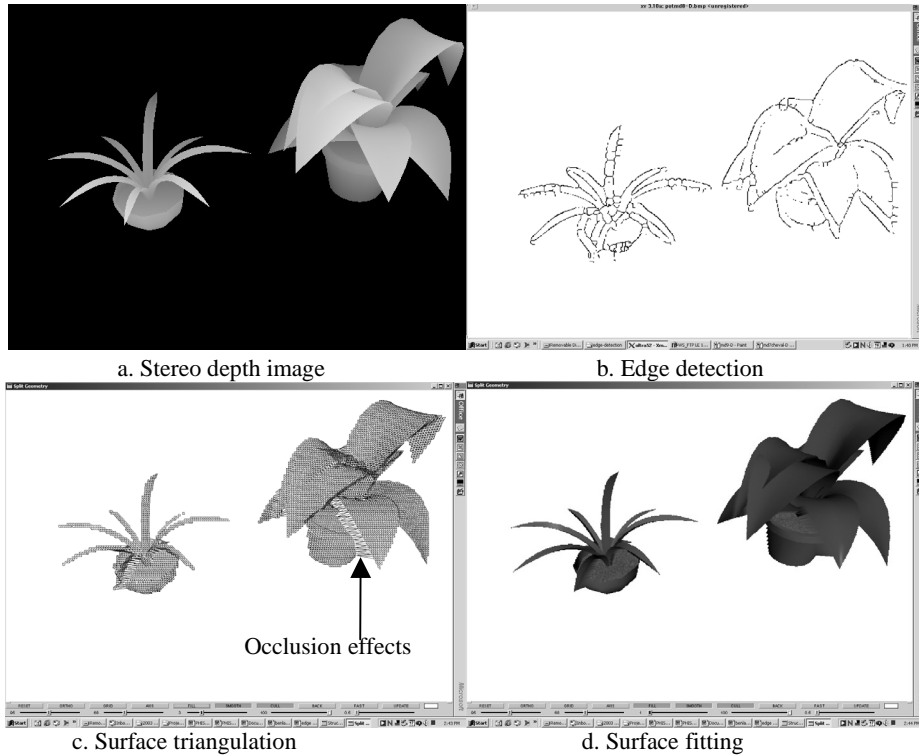


Fig. 5. Surface Fitting Results Showing Occlusion Effects

5 Conclusion

A new technique for 3-D surface segmentation of free-form objects using algebraic implicit surfaces is presented. This technique is based on piecewise hermite interpolation surfaces which are propagated and blending to reduce the number of used surface patches. The proposed technique also preserves surface orientation and depth continuity by using information extracted from the edge map. The technique has been tested using noisy synthetic data and real range images. The experimental results have shown that reliable 3-D surface description of the scene can be reconstructed. However, the surface triangulation technique has been found to be sensitive to occlusion effects resulting from edge detection. Further research work is underway to investigate occlusion effects.

References

1. Ernest, M. and Wu, S.Y.: Surface Parameterization and Curvature Measurement of Arbitrary 3D Objects: Five Practical Methods. *IEEE Trans. PAMI*. Vol.14 (1992) 833-840.
2. Campbell, R.J. and Flynn, P.J.: A Survey of Free-Form Object Representation and Recognition Techniques. *Comp. Vision and Image Understanding*. **81** (2001) 66-210.
3. Fan, T.J.: *Description and Recognizing 3-D Objects Using Surface Properties*. Springer-Verlag. (1990).
4. Zhang, Y.J.: Evaluation and Comparison of Different Segmentation Algorithms. *Pattern Recognition Letters*. Vol.18 (1997) 963-974.
5. Lee, K., Meer, P. and ParkL, R.: Robust Adaptive Segmentation of Range Images. *IEEE Trans. PAMI*. Vol.20 (1998) 200-205.
6. Baccar, L. and Gee, L.A.: Segmentation of Range Images Via Fusion and Morphological Watersheds. *Pattern Recognition*. (1996) 1673-1686.
7. Yokoya, N. and Levine, M.: Range Image Segmentation Based on Differential Geometry: A hybrid Approach. *IEEE Trans. PAMI*. Vol.11 (1989) 643-649.
8. Benlamri, R.: Range Image Segmentation of Scenes with Occluded Curved Objects. *Pattern Recognition Letter*, Vol.21 (2000) 1050-1061.
9. Ma, W.Y. and Manjunath, B.S.: Edge Flow: a Technique for Boundary Detection and Image Segmentation. *IEEE Trans. Image Processing*. Vol.9 (2000) 1375-1388.
10. Dierck, P.: *Curve and Surface Fitting with Splines*. Oxford Science. (1993).
11. Farin, G.: *Curves and Surfaces for CAGD*, 4 Ed. Academic Press San Diego (1997).
12. Subrahmonia, et al.: Practical Reliable Bayesian Recognition of 2-D and 3-D Objects using Implicit Polynomial and Algebraic Invariants. *IEEE Trans. PAMI*. Vol.18 (1996) 505-519.
13. Taubin, J.: Estimation of Planar Curves, Surfaces and Non-planar Space Curves, Defined by Implicit Equations with Applications to Edge and Range Image Segmentation. *IEEE Trans. PAMI*. Vol.13 (1991) 1115-1138.
14. Raja, N.S. and Jain, K.: Recognizing Geons from Superquadrics Fitted to Range Data. *Image Vision Computing*. Vol.10 (1992) 179-190.
15. Ayong-Chee, N. et al.: A Hybrid Approach to 3-D Representation. in *Object Representation in Computer Vision II*. Springer-Verlag. Berlin. (1996) 321-333.
16. Tasdizen, T., Tarel, J.P. and Cooper, D.B.: Improving the Stability of Algebraic Curves for Applications. *IEEE Trans. on Image Processing*. Vol.9 (2000) 405-416.
17. Bajaj, C. et al.: Modeling with Cubic A-patches. *ACM Trans. Graphics*. Vol.14 (1995) 103-133.
18. Alboul, L. and van Damme, R.M.J.: Polyhedral Metrics in Surface Reconstruction: Tight Triangulations. In *Mathematics on Surfaces VII*, T.N.T. Goodman Ed., (1997) 309-336.
19. Gao, X. and Li, M.: Construct Piecewise Hermite Interpolation Surface with Blending Methods. *Proc of 2nd Int. Conf on Geometric Modeling and Processing*. IEEE Computer Society Press. Wako Japan. (2002) 53-59.
20. Hartmann, E.: Implicit G^1 -Blending of Vertices. *Computer Aided Geometric Design*. **18** 267-285.